China SV2 (SuperView Neo-2) X-band SAR support within GAMMA Software

Urs Wegmüller, Christophe Magnard, Charles Werner, Gamma Remote Sensing AG

Version 12-Jun-2025

1. INTRODUCTION

In this document the support provided in the GAMMA Software for the processing of data of the Chinese X-band SAR SV2 (SuperView Neo-2, sometimes also named SuperView-2 or Gaojing-2) is summarized. A first version was written in Nov. 2023. This version was updated in May/June 2025 with additional examples. The main updates, compared to the Nov. 2023 version, are:

- Precision orbits and Calibration parameters are provided with the SV2 SLC data (and a program was implemented to copy the precision state vectors into the SLC parameter file)
- The reader program was slightly updated to accommodate small changes to the meta data
- We found that estimating Doppler parameters based on the data (using GAMMA programs) is necessary in some cases (in particular for the Spotlight mode data we analyzed) to avoid low quality when resampling or oversampling the SLC)

China Siwei is planning to build 28 RS commercial satellites system before 2025, with 16 high resolution (0.2-0.3m resolution) optical satellites, 4 wide-width (0.7m resolution + 100km swath width) optical satellites and 8 SAR (X-band, 0.5m resolution) satellites to obtain the capacity of high resolution, wide-width, various sensors, fast receiving, and global coverage.

In Aug. 2022, the first two X-band SAR satellites for this constellation were successfully launched [https://www.chinasiwei.com/zgswen/Company1/SuperViewconstellation/list/SuperViewconstellation.html]. Superview Neo-2 01/02 are China Siwei's 1st generation SAR sensors. A reflector antenna is used for these sensors. The use of Superview Neo-2 01/02 is more focused on military applications and testing.

Superview Neo-2 03/04 were launched in Nov 2024. Superview Neo-2 03/04 is the second generation SAR system using Phase Array antenna, quite similar to TerraSAR-X / Tandem-X. Superview Neo-2 03/04 are purely for commercial market and will be complemented in the end of 2025 by Superview Neo-2 05/06 which are consistent and can be combined with Superview Neo-2 03/04.

In Section 2 the importing of the SuperView Neo-2 SAR SLC data is described, followed by an assessment of the data characteristics, in Section 3. In Section 4 a SuperView Neo-2 Spotlight mode SLC is investigated. In Section 5, the DInSAR processing sequence for repeat pass interferometric SV2 data pairs is presented. In Section 6, tandem pairs consisting of a mono-static reference scene and a corresponding bistatic second scene are interferometrically processed. The main result generated is a terrain height correction relative to a pre-existing DEM. Besides, the coherence is found of interest for landuse classification and the retrieval of geo- and bio-physical parameters.

2. IMPORTING SV2 SLC DATA

2.1. Importing SLC data

SV2 SLC data are provided as a GeoTIFF with meta data in XML format, that can be read / imported using the program ***par_SV2_SLC***.

par_SV2_SLC SV2-03_MONO_KSBJ71_STRIP_004488_W70.6_S17.2_20230505_SLC_HH_L1A_0000129900.tiff SV2-03_MONO_KSBJ71_STRIP_004488_W70.6_S17.2_20230505_SLC_HH_L1A_0000129900.meta.xml 20230505.slc.par 20230505.slc 0

As input, the GeoTIFF and the meta data XML files are indicated. The program generates the SLC binary data file, in SCOMPLEX or FCOMPLEX format, and the related SLC parameter file. The SLC can be visualized using

disSLC 20230505.slc 10612 1 32000 1. .35 0

and the spectrum can be checked using

dismph_fft 20230505.slc 10612 1 0 1. .35 128 3 0 &

The orbit state vectors appear not "noisy" but there is a jump in the correction from positive to negative values. Most likely, the state vectors correspond to post-processed GNSS measurements. Using the program *ORB_filt_spline.py* the state vector quality can be checked / improved.

/bin/cp 20230505.slc.par 20230505.slc.par.orig

ORB_filt_spline.py 20230505.slc.par.orig 20230505.slc.par.tmp --png png_dir --degree 5

The statistics show centimeter scale standard deviation of the unfiltered state vector positions from the filtered solution. The generated PNG file with the positional deviations is shown in Figure 1.

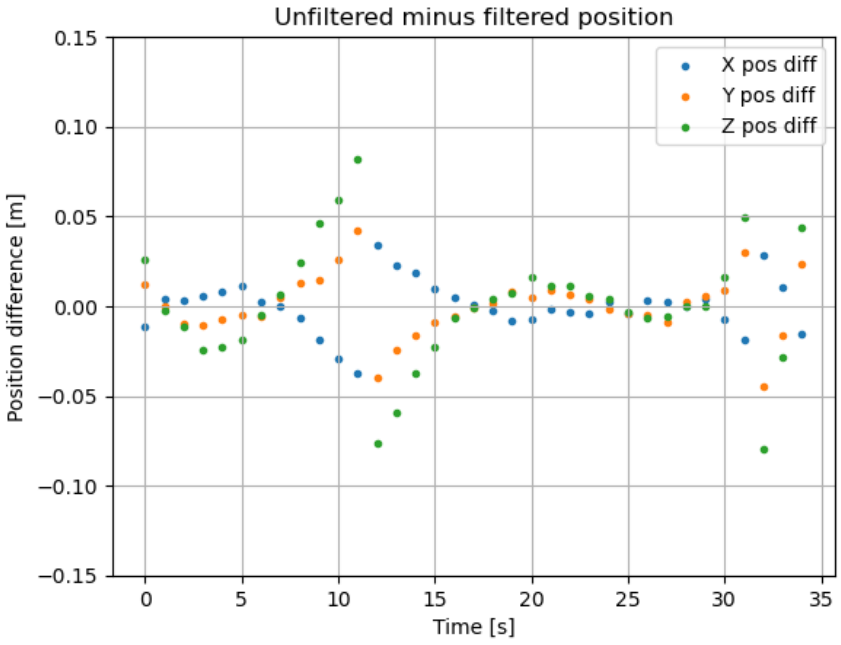


Figure 1 State vector deviations from the filtered solution. There are cm-scale position deviations between the filtered and unfiltered solutions.

We replace the state vectors with filtered state vectors and avoid using the state vectors at the end of the sequence to avoid the outliers. As a result, we obtain the updated 20211221.slc.par.

Using the SLC we generate a backscatter image in slant range geometry using *multi_look* and visualize it using *ras_dB* and *disras*.

A section of the resulting SV2 backscatter image is shown in Figure 2.

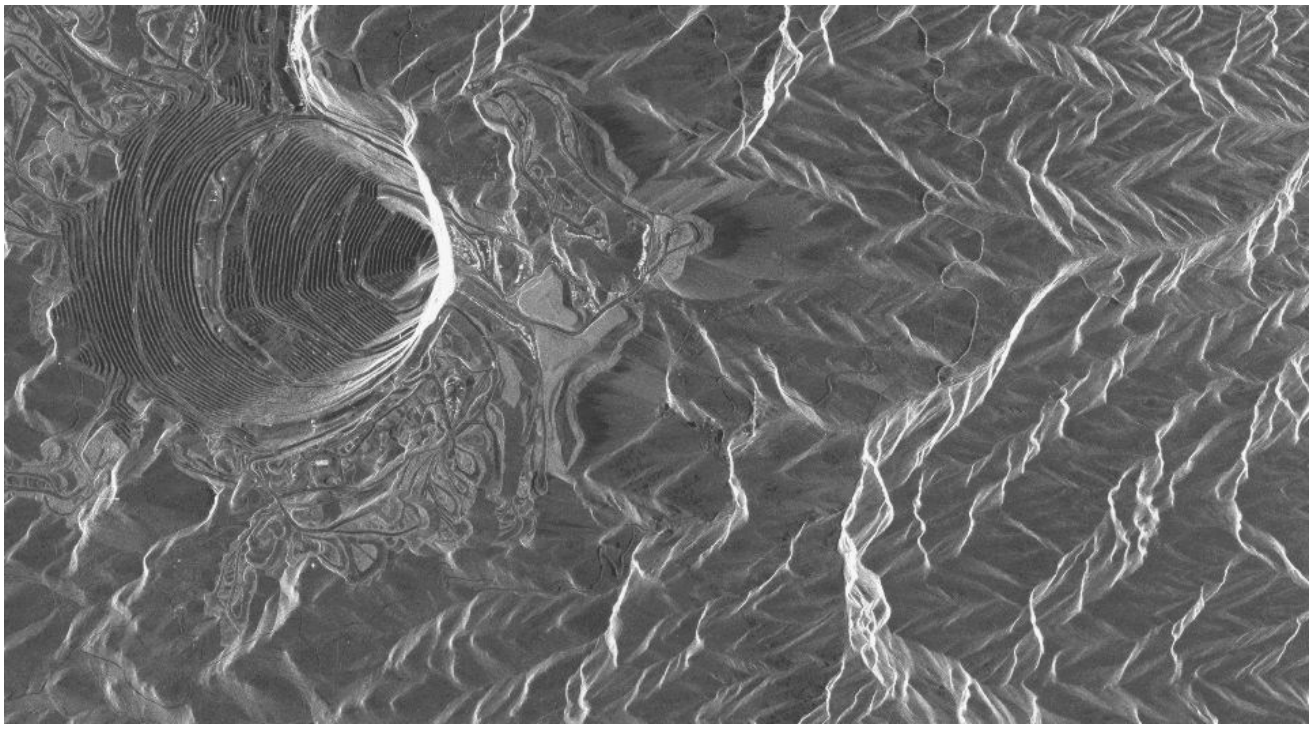


Figure 2 Section of SV2 data (5 x 5 look MLI in slant range geometry).

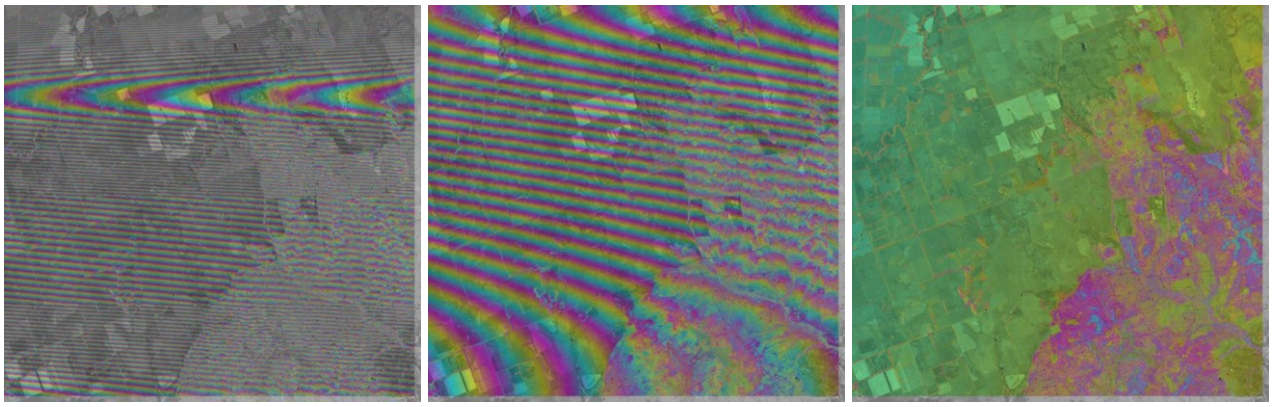
2.2. Precision state vectors

For newer SV2 SLC data precision state vector files are provided together with the SLC data and meta data. The program SV2_precision_orbit.py (available from mid-2025 release) can be used to extract the relevant precision state vectors and write those into the SLC parameter file:

*SV2_precision_orbit.py 20241225.slc.par ../inputs_20250516/20241225/*ABSORBIT_SCIE.xml*

Applying *ORB_filt_spline.py* to the SLC parameter file with the precision state vectors results in a very small standard deviation (<< 1mm) between filtered and unfiltered state vectors, confirming that the precision state vectors were successfully added.

It is strongly recommended to use the precision state vectors to avoid reduced quality co-registration and phase anomalies in interferograms. Figure 3 shows for a bistatic (Tandem) acquisition the differential interferogram (without detrending) obtained using the unfiltered state vectors, the filtered state vectors and the precision state vectors.



unfiltered state vectors filtered state vectors precision state vectors

Figure 3 Differential interferograms for a bistatic (Tandem) acquisition (using SVN2-03 and SVN2-04) on 20250208 calculated using the unfiltered state vectors from the meta data (left), the filtered stated vectors (center) or the precision state vectors (right). One color cycle corresponds to one phase cycle. The subtracted topographic phase was estimated based on the 30m Copernicus DEM.

2.3. Importing detected data in slant range geometry

Not available so far.

2.4. Importing geocoded / georeferenced data

Not available so far.

3. ASSESSMENT OF SOME CHARACTERISTICS OF SV2 STRIPMAP SLC

3.1. Radiometric calibration and estimation of NESZ

With the mid 2025 release the reader program was updated and now considers the radiometric calibration information available in the meta data. For the newer stripmap mode SLC sample data, this results in a radiometric calibration that looks correct. For older data or when using an older version of the reader program a scaling can be applied in the *multi_look* step to bring the backscatter to reasonable values. No validation with different satellite data or targets with known backscatter coefficients was done in our assessment.

Using dark areas (radar shadow and smooth water surfaces) we estimated a Noise Equivalent Sigma Zero value. Although a precise radiometric calibration was not applied – introducing some uncertainty – the results still indicate that the NESZ is relatively low (< -18 dB).

3.2. Point target characteristics

Considering several small, strong scatterers present in the scene we determined the following point target characteristics (for a Fine-Spotlight mode scene of SV2-04):

slant range resolution (3dB):	0.28 m
azimuth resolution (3dB):	0.39 m
peak_side_lobe_ratio:	< -20 dB

3.3. Geocoding

We generated a multi-look intensity image using 5 range and 5 azimuth looks and conducted a geocoding sequence, using the 1-arc-second Copernicus DEM. As part of the geocoding sequence a refinement was determined based on the offset between a simulated backscatter image (calculated based on the orbit data and the DEM) and the actual SAR backscatter.

The refinement statistics indicate for the offset estimates a very small standard deviation of below 0.2 multi-look pixel in both slant range and azimuth directions. For the data acquired in 2023, the determined range and azimuth offsets were also small (< 2m). A geocoded backscatter image is shown in Figure 3. Because of the mountainous terrain a large fraction of the area is in layover.

3.4. RFI filtering

The provided sample data was not affected by Radio-Frequency-Interference (RFI), which causes ghost images, zones with significantly increased noise, etc. Hence no RFI filtering was necessary.

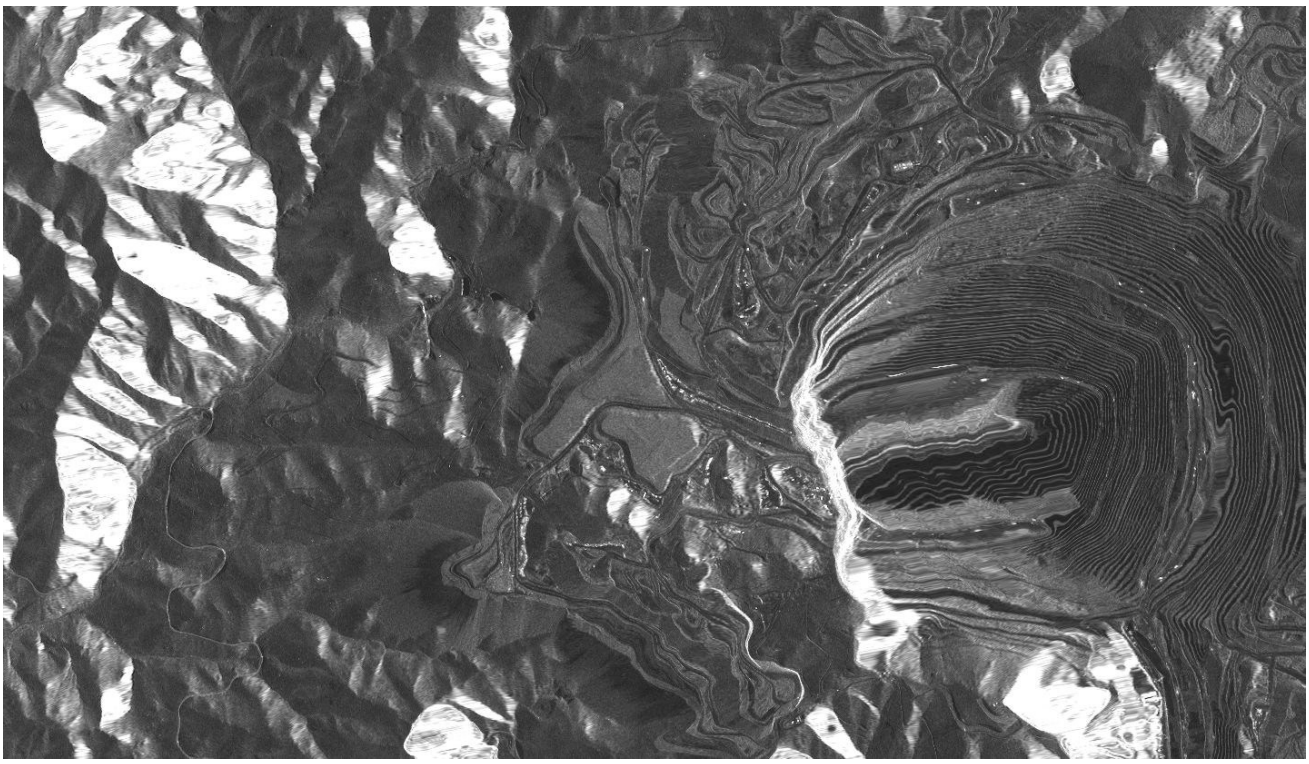


Figure 3 Section of a geocoded SV2 backscatter image over Chile.

4. SPOTLIGHT MODE SV2 SLC

4.1. Azimuth spectrum information estimation from SLC

In our assessment in May 2025, we noticed that the Spotlight mode SV2 SLC data could be read using *par_SV2_SLC*, but no Doppler information was found in the meta data. Checking the spectrum using *dismph_fft* showed that the azimuth spectrum is varying between different parts of the scene. And the azimuth spectrum is not centered, which is problematic when resampling (e.g. in a co-registration) or oversampling the data (assuming the Doppler Centroid is zero). This problem can be overcome by estimating the doppler polynomial based on the SLC data and writing the estimated information into the SLC parameter file using

doppler_2d_SLC 20241213.slc 20241213.slc.par - - 512 - 0 1 1 1

The zero value Doppler polynomials in the SLC parameter file

doppler_polynomial: 0.00000 0.00000e+00 0.00000e+00 0.00000e+00 Hz Hz/m Hz/m^2 Hz/m^3

doppler_poly_dot: 0.00000e+00 0.00000e+00 0.00000e+00 0.00000e+00 Hz/s Hz/s/m Hz/s/m^2 Hz/s/m^3

are replaced with the estimated values

doppler_polynomial: 50.81589 3.99948e-02 0.00000e+00 0.00000e+00 Hz Hz/m Hz/m^2 Hz/m^3

doppler_poly_dot: -9.32996e+03 0.00000e+00 0.00000e+00 0.00000e+00 Hz/s Hz/s/m Hz/s/m^2 Hz/s/m^3

As a test we applied a deramping of the azimuth spectrum using

SLC_deramp 20241213.slc 20241213.slc.par 20241213.slc.deramp 20241213.slc.deramp.par 0

and checked the spectrum of the deramped SLC using

dismph_fft 20241213.slc.deramp 28832 1 - 1. .35 128 3 0

The azimuth spectrum is now centered and constant over the entire image – which confirms that the estimated Doppler values are of good quality. This also means that resampling and oversampling of the Spotlight mode SLC is now possible at high quality.

4.2. Identify and mitigate narrow directional scattering effects using azimuth spectral looks

Some targets, in particular man-made as large flat surfaces (e.g. roofs), dihedral elements (e.g. house-ground), and straight cylinders (e.g. powerlines) cause narrow directional scattering. Such scattering can be disturbing, when interpreting SAR imagery, on the other hand it also provides potentially interesting information on the presence of such targets.

A Spotlight acquisition has a wide azimuth spectrum which permits identifying and mitigating directional scattering. For this we deramp the Spotlight SLC after estimating the Doppler parameters, as shown above. For the deramped SLC we apply azimuth band-pass filtering using the program *bpf*. In our example we generated 8 sub-band images, each one with a sub-band of 0.12 of the sampling band-width. We rescale the sub-band images on similar levels (to account for differences in the related parts of the antenna gain) by adjusting them so that they all have roughly the same average backscatter. Then we calculate the median across the spectral look images using the LAT program

multi_stat im_list 9610 20241213.mli.median 1

The very narrow directional scattering is only present in one or two of the azimuth looks and therefore not in the median of the 8 looks. So in the median image the “directional effects” are “suppressed”. On

the other hand, the ratio between the average image and the median image can be used to highlight the directional scattering effects. Figure 4 and Figure 5 (for a small section) show the median image, the average image and a hue-saturation-intensity image using the average-median ratio for the hue and the saturation and the average image for the intensity.

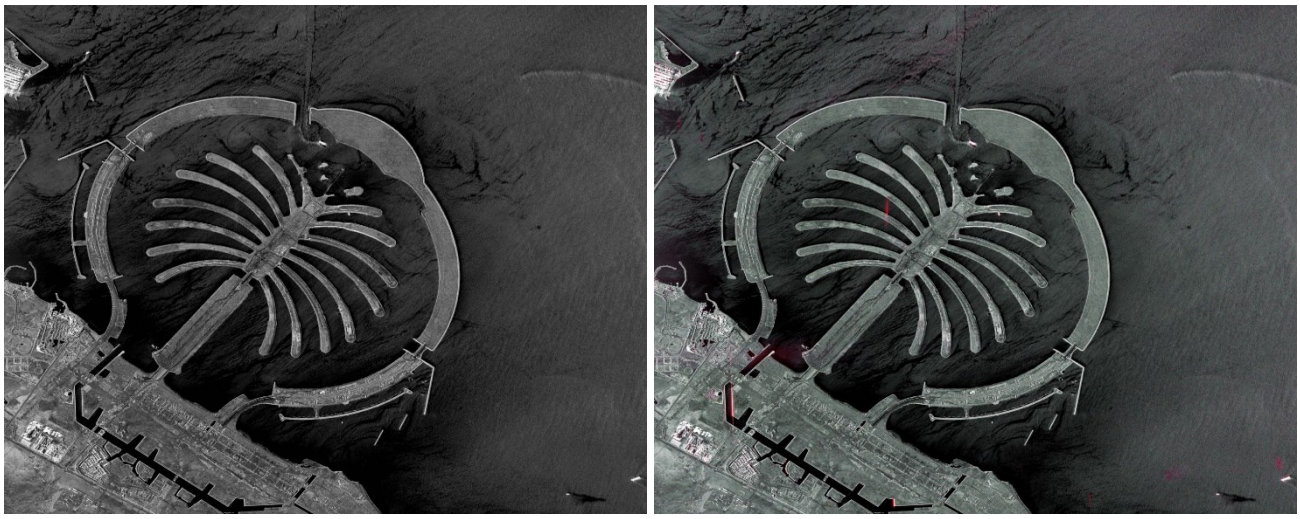


Figure 4 Spotlight SV2 data acquired on 20241213 over Palm Jebel Ali. The left image shows the spectral-looks median image (with narrow directional scattering effects suppressed). The right image shows the HIS composite that highlights the narrow directional scattering effects in red color.

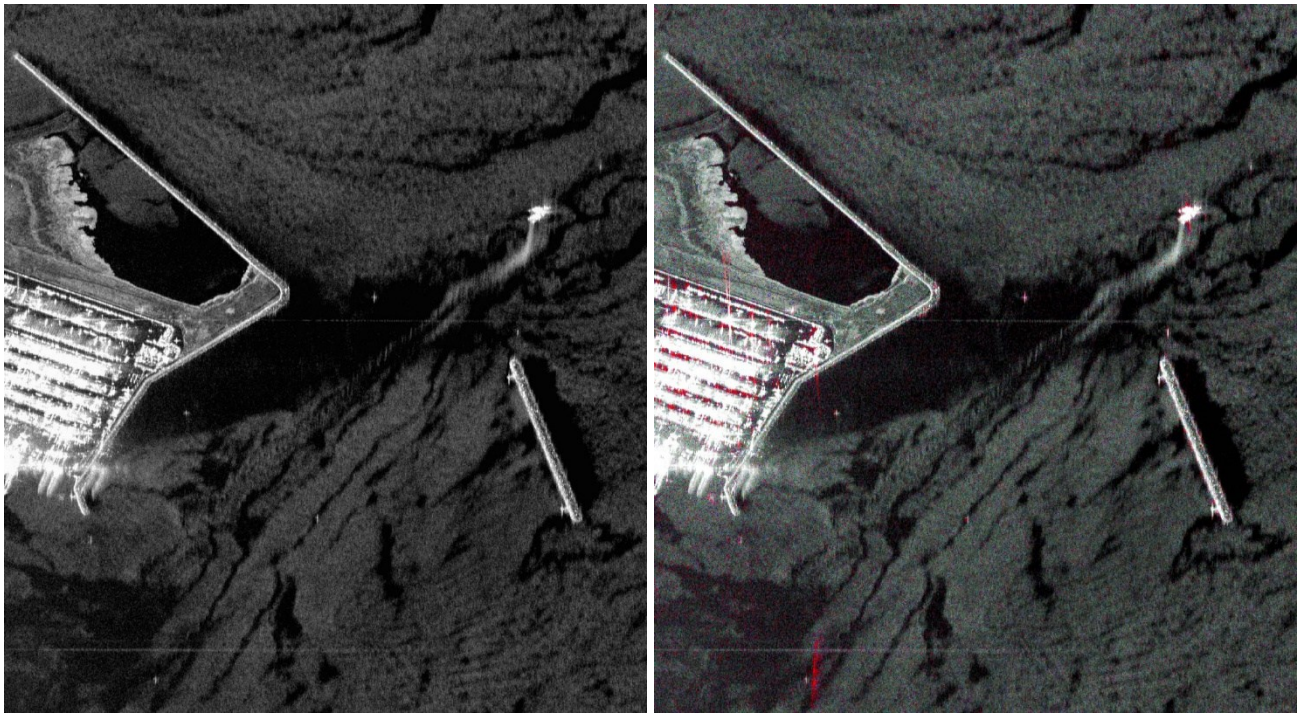


Figure 5 Spotlight SV2 data acquired on 20241213 over the top left of the Palm Jebel Ali area shown in Figure 4. The left image shows the spectral-looks median image (with narrow directional scattering effects suppressed). The right image shows the HIS composite that highlights the narrow directional scattering effects in red color.

5. SV2 REPEAT-PASS DIFFERENTIAL SAR INTERFEROMETRY (DINSAR)

5.1. Processing sequence used and results

We were able to test SV2 differential SAR interferometry using an SV2 pair with 17 days difference and a perpendicular baseline component of about 132m, acquired on 5. and 22. May 2023 over Chile.

A flow chart of the processing sequence used is shown in Figure 6. In the following, some of the steps are further discussed.

The two scenes used were acquired by SV2-01 (second scene, 22. May 2023) and SV2-01 (reference scene, 5. May 2023). The importing of the two SLCs was done using the program *par_SV2_SLC*. After the importing we checked and filtered the orbit state vectors.

We selected then the earlier scene as the reference, generated a multi-look intensity image (MLI) with 5 range and 5 azimuth looks, and conducted a geocoding sequence using the Copernicus 30m global DEM. This also included the resampling of the DEM height into the MLI geometry.

Next, we co-registered the second SLC to the reference SLC. In this we used a sequence that also considers the terrain height (using *rdc_trans*). In this a refinement is done using intensity matching, to achieve a co-registration accuracy better than 0.1 SLC pixel.

Then we calculated the orbital and topographic phase (*phase_sim_orb*) and the differential interferogram (*SLC_diff_intf*). The resulting differential interferogram has a high coherence but shows a quite substantial overall phase trend, mainly in the azimuth direction (Figure 7a). We unwrapped the differential interferogram (*mcf*), estimated the overall phase trend (*quad_fit*, Figure 7b), and subtracted it (*sub_phase*), to get the "detrended" differential interferogram (Figure 7c). Using the precision orbits which are available with the newer acquisitions, estimating and removing an overall trend may not be necessary or only a slight trend needs to be removed.

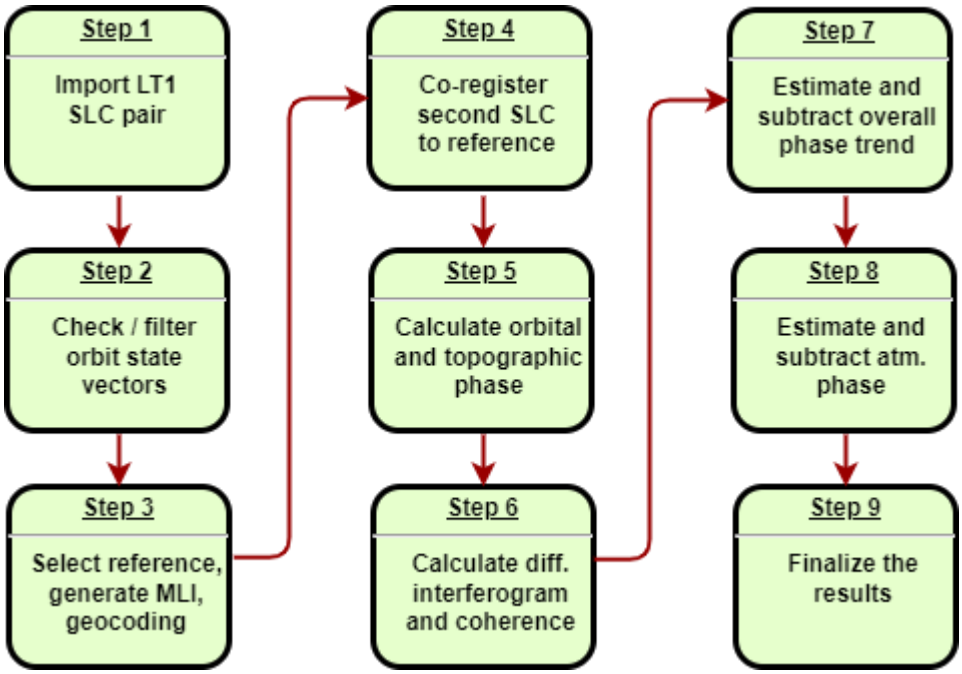
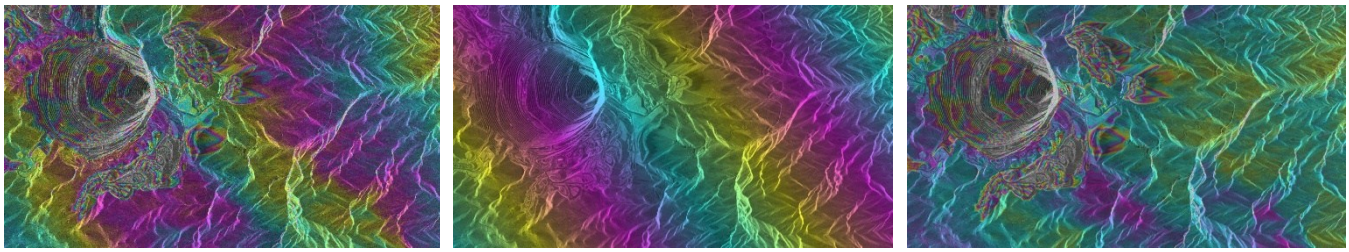
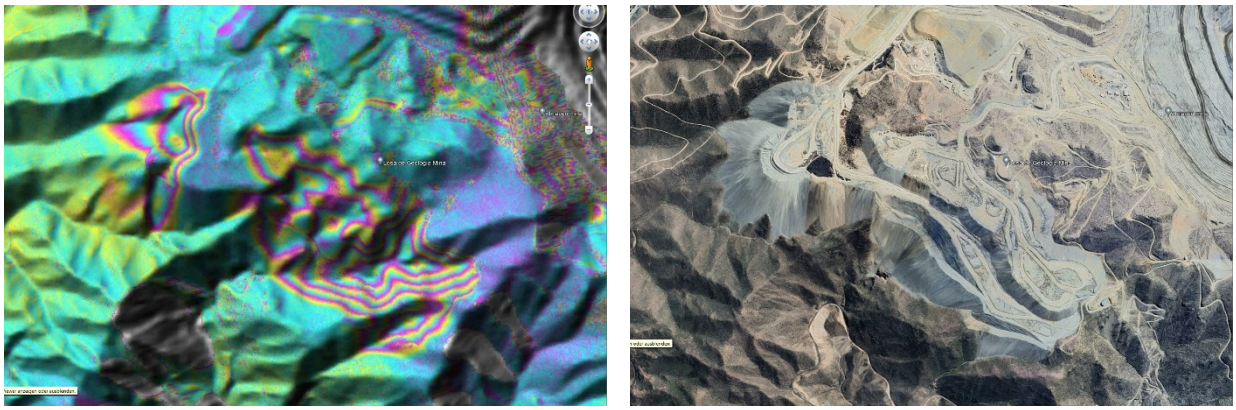


Figure 6 Flowchart of DInSAR processing sequence used.



a) differential interferogram b) estimated trend c) detrended interferogram

Figure 7 "Detrending" of SV2 differential interferogram.



a) differential interferogram b) same area in Google Earth

Figure 8 SV2 differential interferogram. The main phase contribution is topographic phase related to terrain changes from mining activities.

Starting from the "detrended" differential interferogram we would normally estimate an atmospheric path delay. In this example this is difficult because of the presence of strong topographic phases in the mining area present in the scene. Distinguishing deformation phase, atmospheric phase and topographic phase with the single differential interferogram cannot be reliably achieved. Probably most of the phase is topographic phase (Figure 8), but there is also significant atmospheric phase present. To identify displacements in the mining area, further acquisitions or a current high-resolution DEM would be needed.

Another DInSAR example, using Superview Neo2-03 was evaluated, this time with a very short spatial baseline of only 6 meter and a time interval of 16 days, over the Yanya mining area. The underground mining activities cause substantial subsidence at the ground surface (up to more than 20cm over the 16 days). As a result, the complex valued SV2 X-band differential interferogram (Figure 9) shows many phase fringes which complicate phase unwrapping. To get an optimal result we apply an oversampling of the SLC and estimate the differential interferogram using SLC_intf2 with a small spatial decimation while taking looks over a significantly larger area. A first unwrapping clearly shows the deep subsidence cones (with > 10 fringes, Figure 9) but is most likely still underestimating the depth. We therefore apply an iterative sequence to improve the result. We apply a spatial filtering to the first unwrapping result (strong enough to get rid of any phase jumps e.g. from unwrapping ambiguity errors) subtract this phase and iteratively redo this unwrapping, filtering and subtraction sequence. After several iterations we sum up the subtracted components to get our final subsidence estimate. Figure 10 shows the geocoded final result (using two different visualizations).

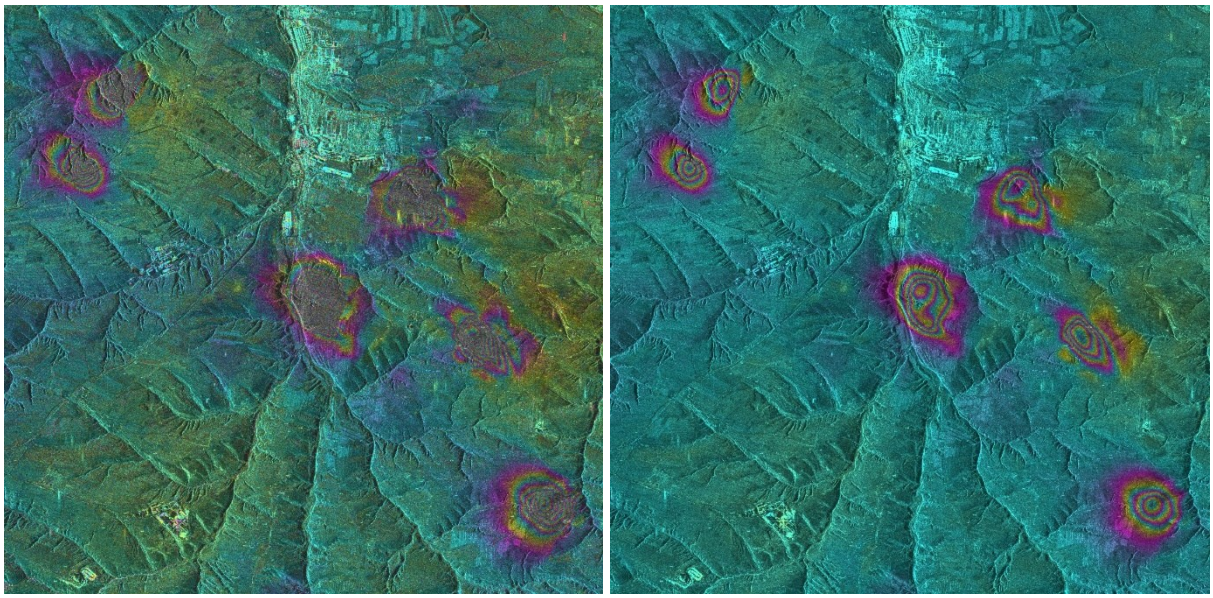


Figure 9 Superview Neo2-03 differential interferogram over Yanya Mining area shown in slant range geometry (20241225_20250110, $B_\perp$ 6m, dt 16 days). The main phase contribution is deformation phase. The image to the left shows the original differential interferogram with a cyclic color scale with one phase cycle per color cycle. The image to the right shows the spatially filtered first unwrapping solution with a cyclic color scale with two phase cycles per color cycle.

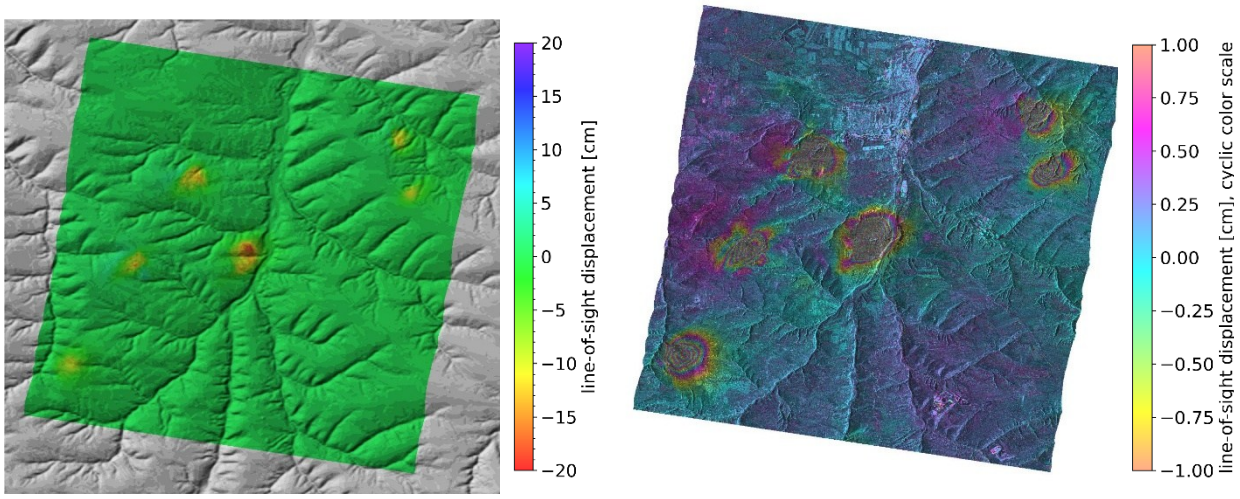


Figure 10 Geocoded line-of-sight displacement map for the SV2 differential interferogram over Yanya Mining of Figure 9, shown on the left side with the shaded relief used as image brightness and on the right sight using the backscatter as the image brightness and using a cyclic color scale with 2cm per color cycle to better visualize the result in the areas with high deformation gradients.

5.2. Discussion

The examples investigated clearly confirm that SV2 can be used for repeat-pass SAR interferometry.

6. SV2 SINGLE-PASS DIFFERENTIAL SAR INTERFEROMETRY (TANDEM-DINSAR)

6.1. RFI filtering

Reading of the bistatic pair is done in the same way as shown in Section 2.1, using *par_SV2_SLC*. Then we check the xml file to determine which of the two scenes acquired by the SV2-03 and SV2-04 is the active one (it is SV2-04 in this case) and use it as the geometric reference.

Checking the data, we see that the bistatic scene received by the SV2-03 shows some anomalies in the near range. Checking the spectrum with *dismph_fft* shows that this is most likely related to the low frequency part of the range spectrum. Applying slight range band-pass filtering

bpf SV2-03_20230131.slc SV2-03_20230131.slc.bpf_filt 23894 0.0 0.4 0.0 0.7 - - - - 0

permits getting rid of this problem. Figure 11 shows for a small section in the near range the original and RFI filtered backscatter image.

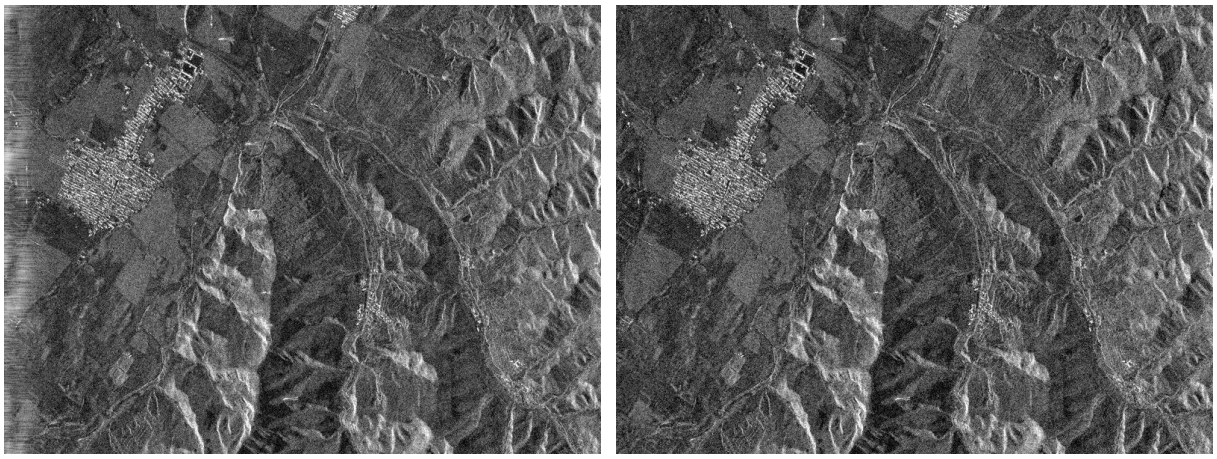


Figure 11 Original (left) and RFI-filtered (right) backscatter image. The anomaly in the near range is removed.

6.2. Processing sequence used

After the launch of SV2-03 and SV2-04 in 2023 the two X-band SAR sensors are operated in a Tandem mode with one sensor transmitting and receiving (monostatic acquisition) and the other one also receiving the signal transmitted by the first (transmitting) sensor (bistatic acquisition). Combining the monostatic and bistatic acquisitions supports single-pass interferometry. Single-pass interferometry with a spatial baseline can be used to determine topographic heights. Examples for this are the SRTM DEM that was generated using single-pass C-band acquisitions and the Copernicus DEM that uses X-band single-pass acquisitions acquired by the Tandem-X satellite constellation.

For our testing we used a single pass SV2-04/SV2-03 tandem pair acquired with a perpendicular baseline component of about -360m, acquired on 31. Jan. 2023.

A flow chart of the processing sequence used is shown in Figure 12. In the following some of the steps are further discussed.

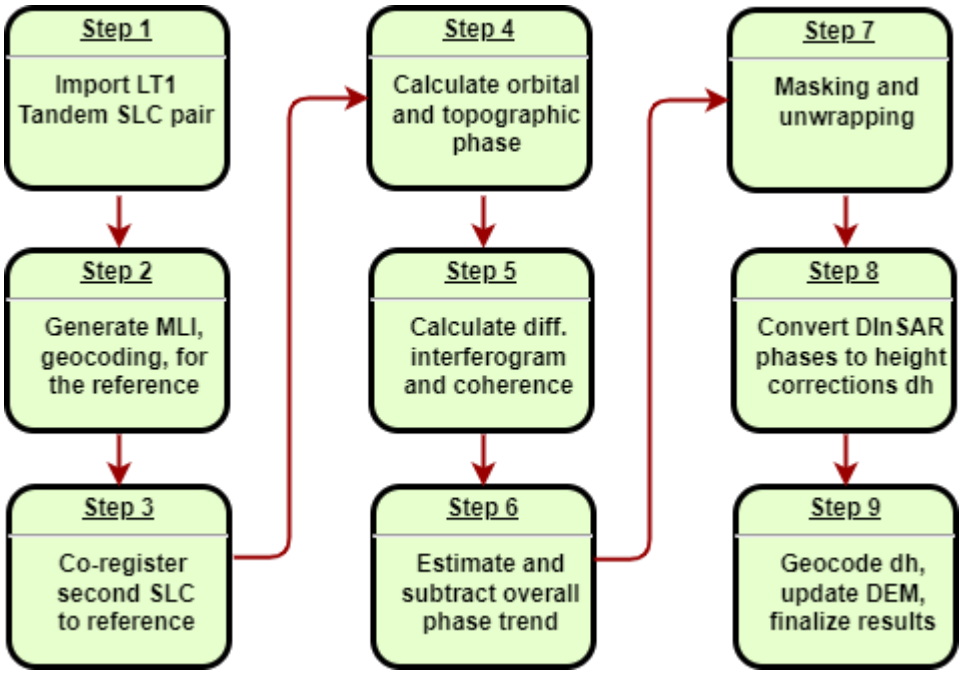


Figure 12 High-level flowchart of DInSAR processing sequence used to update a pre-existing DEM based on a SV2 Tandem pair.

The importing of the scenes is done using the program *par_SV2_SLC*. Importing of the bistatic scene is done in the same way as for the monostatic scene. With the bistatic acquisition, XML files with meta data are provided per data set. In addition, a third XML is provided with a name that includes SV2AB. Among other things this file informs about which one of the two sensors is the monostatic (active) and which one the bistatic (passive) sensor. In our example SV2-04 is the active sensor, so we use SV2-04 as the reference of the single-pass interferometric pair.

As for other SV2 SLC data we recommend to either replace the orbit state vectors by the precision orbit state vectors – when available – using the program *SV2_precision_orbit.py*, or check/filter the orbit state vectors immediately after reading the data (to assure that the filtered state vectors are present e.g. in the MLI parameter file). This checking/filtering is done using the program *ORB_filt_spline.py*. In our example there was for both scenes for one coordinate a saw tooth deviation with a magnitude of about 5cm. We think that this may be related to a quantization issue (not of the state vectors provided with the data but with a previous intermediary element used in the navigation data processing).

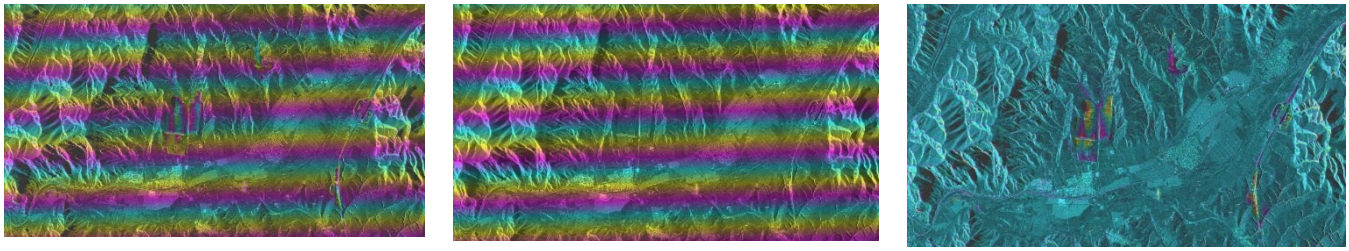
The monostatic scene is selected as the reference, a multi-look intensity image (MLI) with 6 range and 4 azimuth looks is generated, and a geocoding sequence using the Copernicus 30m global DEM is conducted. This also included the resampling of the DEM height into the reference MLI geometry.

In the co-registration of the second scene, which is the bistatic acquisition, to the reference, we have to consider that the second scene is not a different monostatic scene but a bistatic scene. For the bistatic acquisition, the two-way slant range is the sum of the slant ranges from the first orbit to the target (r1) and from the target to the second orbit (r2). So the "effective slant range" is (r1+r2)/2 (and not r2). A co-registration procedure using the older version of *rdc_trans* was implemented in *SLC_coreg_tandem.py*. Starting with the Dec. 2023 release, updated versions of *rdc_trans* and *SLC_coreg.py* with a "tandem mode option" are available in the software.

In the co-registration of a pair with a long spatial baseline, considering the terrain topography effects is relevant. Using a constant height instead of a DEM or using a DEM with significant errors may result in imperfect co-registration. Co-registration errors > 0.2 pixel in slant range result in a reduction of the coherence, errors > 1 pixel may result in a complete decorrelation. Doing the processing without a DEM, assuming a constant height, seems reasonable. A refinement step would then be applied based on an offset field estimated using *offset_pwr_tracking*.

After the co-registration, the simulation of the orbital and topographic phase is done using *phase_sim_orb*. Here it is important that the "single-pass mode" is used. Using the co-registered SLC and the simulated orbital and topographic phase we can then calculate the single-pass differential interferogram (using *SLC_diff_intf*). For a single-pass interferogram there is no temporal decorrelation, so we expect that the coherence is very high. Low coherence is observed for layover and shadow areas, for areas with very low backscatter (e.g. smooth water surfaces and wet snow). Non-overlapping parts of the reflectivity spectra may also reduce the coherence (depending on the perpendicular baseline component) and for areas with significant volume scattering the coherence may also be reduced (by "volume decorrelation"), again depending on the length of the perpendicular baseline component.

For the SV2 single-pass differential interferogram it was necessary to estimate and subtract an overall phase trend (possibly related to orbit errors or processing effects, Figure 13).



a) differential interferogram b) estimated trend c) detrended interferogram

Figure 13 "Detrending" of SV2 Tandem differential interferogram.

After getting the detrended single-pass differential interferogram, the phase needs to be unwrapped. In layover/shadow areas, and very close to such areas, the phase is very noisy. It is recommended to mask layover and shadow areas as well as areas with low coherence. The resulting area can be unwrapped using *mcf*, or if phases are all in the interval (-π,π) using *cpx_to_real*. The phase values can then be converted to height corrections using *dh_map_orb*. With a perpendicular baseline of -360m the phase to height sensitivity of the single-pass DInSAR phase is about 0.133 radian/meter (respectively 7.52 meter/radian). The topographic phases observed (Figure 14) are very plausible, as they are in a mining area.



Figure 14 Topographic phases (corresponding to height correction up to about 25m) are located in an area where Google Earth images suggest that terrain changes happened (mining, land fill).

Next, the height corrections need to be geocoded from the slant-range MLI geometry to the map geometry. Using the lookup table calculated in the normal geocoding sequence (using the available external DEM, i.e. uncorrected heights) is not precise. The new, corrected DEM heights now available in the slant-range MLI geometry should be used. This is possible using the program *gc_insar*. The calculated lookup table is in the dimension of the slant-range MLI image and the values correspond to the corresponding locations in the map geometry. A refinement of the lookup table can be done by resampling the MLI to the map geometry and determining offset parameters using a matching procedure of the transformed MLI and the previously geocoded backscatter using the DEM.

The single-pass example investigated clearly confirms the successful operation of the SV2-03/04 as a constellation. The bistatic scene, the related meta data, and the resulting X-band Tandem interferogram are of good quality. The processing sequence confirms that updating of a pre-existing DEM can be achieved.

To achieve a high quality DEMs over an area in a robust manner, it would be necessary to use multiple Tandem pairs including both ascending and descending orbit. With a single orbital direction, the spatial coverage in mountainous areas is limited by layover and shadow effects.

6.3. Investigation of a more recent SVN2-03 – SVN2-04 Tandem acquisition

In May 2025 we could carry out an additional bistatic InSAR test using a more recent SVN2-03 – SVN2-04 Tandem acquisition over Condamine, Australia. For this acquisition, precision orbit state vectors were available for the two satellites. As a result, the differential interferogram did not have a strong overall phase trend. The Copernicus 30m DEM was used as height reference. The differential interferogram calculated is shown in Figure 15, together with the slight overall trend estimated (considering only the non-vegetated areas with high coherence), and the corrected differential interferogram.

Based on differential interferometric phase relative height corrections were determined. Over the vegetation the coherence was reduced, but still high enough to estimate height corrections. Figure 16 shows the estimated height corrections.



Figure 15 SVN2 X-band bistatic differential interferogram of 20250224 over Condamine, Australia. The image to the left shows the initial differential interferogram, the image in the center the estimated overall slight phase trend and the image to the right the phase trend removed differential interferogram – all using a cyclic color table with one phase cycle per color cycle. The perpendicular baseline of the pair is 634m. As topographic reference the Copernicus 30m DEM was used.

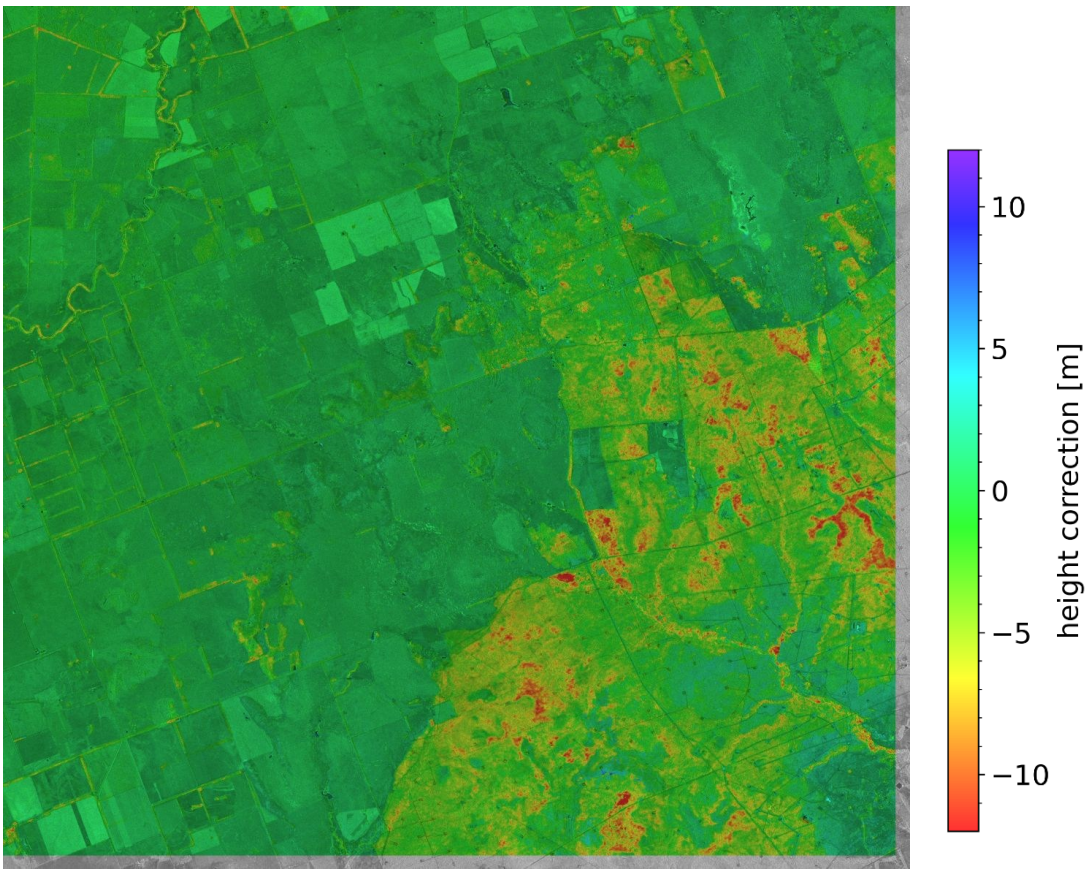


Figure 16 Estimated height corrections (relative to the Copernicus 30m DEM heights used in the calculation of the differential interferogram).

The estimated height corrections are primarily negative, indicating that the height estimated with the SV2 Tandem data is lower than the Copernicus DEM height. Updating the reference height used (Copernicus DEM height) with the determined height correction shows that the corrected heights for forested areas are close to the heights of the surrounding unforested terrain – while the Copernicus DEM heights (also generated from bistatic X-band data acquired by TerraSAR-X and Tandem-X) show heights about 10m higher than the height of the surrounding terrain (Figure 17). The shorter spatial baseline of the Tandem-X data used to generate the Copernicus DEM is the plausible explanation for this difference. The perpendicular baseline of the SV2 bistatic pair is 634m. As a result, the coherence of the scattering from the tree elements above the ground decorrelate so that the coherent part of the signal coming from the ground dominates the interferometric phase. The vegetation is quite sparse in the Condamine area.

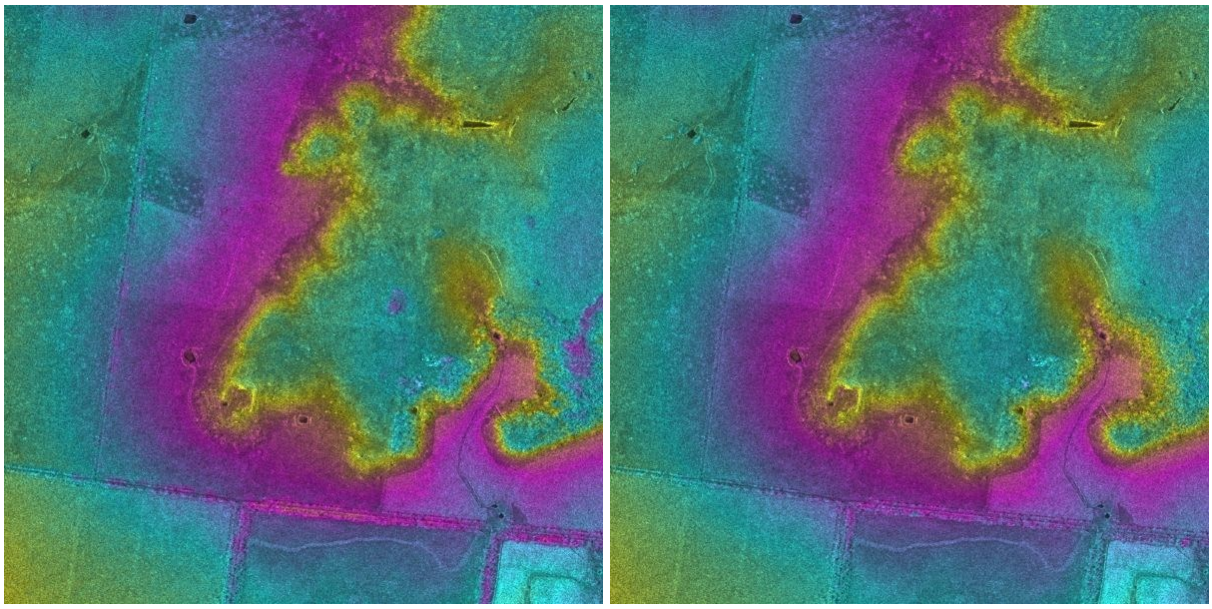


Figure 17 Copernicus DEM height (left) and SV2 data based height (right) for a small section of the area, shown using a cyclic color table with 24m per color cycle. In the Copernicus DEM the height of lines of trees along roads and field boundaries have an increased height. The SV2 based height in the same areas is close to the height of the surrounding unvegetated area.

The reduced coherence for the forested areas can be used as an indicator for forest. Figure 18 shows for the bistatic SV2 acquisition over Condamine the Tandem coherence product. The coherence is clearly reduced for forested area. The reduced value levels in the red channel (showing the coherence) result in a green appearance of the composite. Consequently, the bistatic acquisitions may also be of interest for landcover mapping and the retrieval of bio- and geophysical parameters.

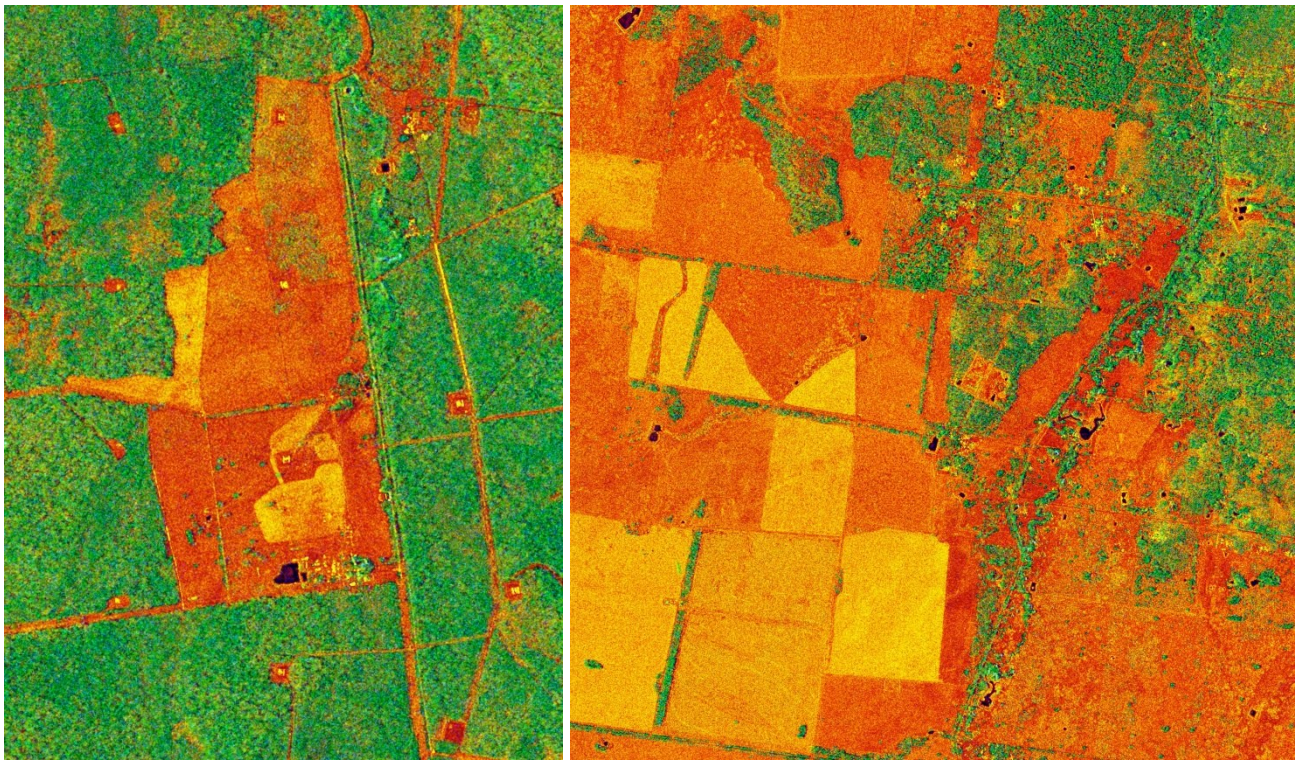


Figure 18 SVN2-03/04 Tandem coherence product for small section of the bistatic acquisition over Condamine, Australia. The coherence product is an RGB composite of the bistatic coherence (red channel, here with a 634m baseline), the average backscatter (green), and the backscatter ratio of the monostatic and bistatic acquisition (blue).

7. ACKNOWLEDGMENT AND COPYRIGHTS

China Siwei Surveying and Mapping Technology Co. Ltd. is acknowledged for providing us access to the data used in our investigation. For more information on the Superview constellation please see: www.chinasiwei.com/zgswen/Company1/SuperViewconstellation/list/SuperViewconstellation.html.